Observation of Raman scattering by cloud droplets in the atmosphere

S. Harvey Melfi, Keith D. Evans, Jing Li, David Whiteman, Richard Ferrare, and Geary Schwemmer

In a recent field campaign, the NASA Goddard Space Flight Center scanning Raman lidar measured, in the water vapor channel, Raman scattering from low-level clouds well in excess of 100% relative humidity. The excess scattering has been interpreted to be spontaneous Raman scattering by liquid water in the cloud droplets. A review of research on Raman scattering by microspheres indicates that the technique may provide a remote method to observe cloud liquid water. The clouds studied appear, from Mie scattering, to have two distinct layers with only the upper layer showing significant Raman scattering from liquid water in the droplets. © 1997 Optical Society of America

1. Introduction

Over the past ten years, Raman lidar has become a powerful tool to study the atmosphere. The technique has been used to measure the vertical structure of water vapor and its temporal variation,[1–5] unattenuated aerosol backscatter profiles,[6] aerosol optical depth,[6] and atmospheric temperature profiles.[7–10] In this paper we report on the observation of Raman scattering by liquid water in cloud droplets.

Laboratory investigations have reported the observation of both spontaneous[11,12] and stimulated[13–17] Raman scattering from water droplets. Stimulated Raman scattering requires a laser intensity several orders of magnitude higher than the intensity of our laser beam. Thus we assume that the observations reported here are due to spontaneous Raman scattering. To first order, we expect that spontaneous Raman scattering by a size distribution of water droplets will be proportional to the total number of liquid water molecules, modified by the spherical shape of the droplets. The dominant shape effects, which are discussed below, tend to increase the Raman backscatter (180°) cross section of the droplets when compared with bulk liquid water. Raman scattering by cloud droplets may provide a new method to remotely measure the liquid water content of clouds, and, along with an independent measurement of conventional Mie scattering, might lead to an inference of cloud droplet size distribution and cloud droplet density.

Cloud droplet size distribution and the number density of cloud droplets may have an important influence on atmospheric radiative transfer. Charlson *et al.*[18] have shown that, as the number of cloud particles increases, due to the higher number of condensation nuclei produced by fossil fuel burning, the reflectivity of these clouds in the visible increases, thus leading to an overall cooling of the Earth–atmosphere system. The cooling may in part counteract the expected warming that is due to increased atmospheric CO_2 that is also attributable to fossil fuel burning. An increase in the cloud droplet number density leads to, in general, smaller-sized droplets; thus the total liquid content of clouds and the number and size distribution of cloud droplets may each be important in evaluating man's impact on the future state of the Earth's climate.

This paper is organized as follows: Section 2 provides a brief overview of the Raman lidar system used in the investigation; this is followed by a description of the experiment and a presentation of the results in Section 3. Section 4 presents a summary of theoretical and laboratory investigations of Raman scattering by droplets; we then provide a discussion of the results of the investigation comparing our observations with our understanding of Raman scattering by

The authors are members of the Raman Lidar Team, NASA Goddard Space Flight Center, Greenbelt, Maryland 21250. S. H. Melfi and J. Li are also with the Department of Physics, University of Maryland Baltimore County, 1000 Hilltop Circle, Baltimore, Maryland 21250. K. Evans and R. Ferrare are also with Hughes STX, Lanham, Maryland 20706.

Received 4 April 1996; revised manuscript received 5 November 1996.

0003-6935/97/153551-09$10.00/0

droplets in Section 5. Section 6 summarizes the study and provides our conclusions.

2. Description of the Raman lidar

The NASA Goddard Space Flight Center scanning Raman lidar has been described by Ferrare *et al.*[6] It was designed to simultaneously measure Raman scattering in the atmosphere by nitrogen, oxygen, and water vapor, as well as Rayleigh (molecular) and aerosol and cloud scattering at the laser wavelength. Raman scattering is a weak scattering phenomenon. The scattered radiation is shifted in frequency from the incident radiation by an amount unique to the scattering molecule.

The lidar consists of a XeF laser that produces radiation in three closely spaced lines centered at 351.1 nm.[19] The other two lines are located at 348.8 and 353.2. The laser output is a continuous series of short pulses (15 ns) at 400 Hz with an average power of approximately 12 W. The optical axis of the laser is aligned with the axis of a 0.76-m Dall–Kirkham telescope. Both the laser and the telescope point out the rear of an environmentally controlled van toward a large pointable mirror that is affixed on a rotatable shaft at a 45° angle. The scattered radiation from the laser pulse, as it propagates through the atmosphere, is also directed by the large pointable mirror into the telescope. The output of the telescope is fed through a field-limiting stop and then divided into four detector channels by several dichroic beam splitters. The channels are made sensitive to the elastic scattering from molecules and aerosols and clouds at the laser wavelength and the Raman scattering from nitrogen, oxygen, and water vapor by specially manufactured interference filters. The Raman filters, similar to the ones described by Whiteman *et al.*,[3] were constructed with very high blocking (10^{-12}) at the laser wavelength. Because the XeF excimer laser has three lines at 348.8, 351.1, and 353.2 nm, we used spectrally wide filters in selecting the Raman bands of interest. Each filter was manufactured to be 7–8 nm wide so as to pass Raman scattering from the three output lines of the laser. Each detector channel was divided further by another beam splitter (95–5%) into two photomultiplier tubes (PMT's) so that atmospheric measurements can be made from near the surface to an altitude of approximately 5 km on the low-sensitivity PMT (avoiding saturation from the high near-field scattering) and from approximately 3 km on up with the high-sensitivity PMT. Thus we use eight PMT's to look at complete altitude profiles at the four wavelengths.

The output of each PMT is amplified and presented to a scaling photon counter. The counter acquires photon counts in successive 0.5-μs bins synchronized with the laser pulses. The data system accumulates counts in these bins from typically 23,200 laser shots before storing the accumulated result. At 400 Hz it takes approximately 1 min to accumulate data from 23,200 laser shots. Thus we obtain a profile at the four wavelengths as a function of range once every minute with a range resolution of 75 m (0.5 μs).

In clear conditions, the ratio of the water vapor return to the nitrogen return (Raman scattering ratio), after a small differential attenuation correction, has been shown by Melfi[20] to be proportional to the water vapor mixing ratio. The water vapor mixing ratio is an important meteorological measure of atmospheric moisture and is defined as the ratio of the mass of water vapor in a volume of air to the mass of dry air in that same volume. The ratio of the backscattered return at the laser wavelength to the nitrogen return (elastic-scattering ratio), again after a small attenuation correction and after normalization to unity in a clean region of the atmosphere, has also been shown by Melfi[20] to be proportional to the aerosol scattering ratio. Whiteman *et al.*[3] and Ferrare *et al.*[6] provide more detail on computing the atmospheric profiles of water vapor mixing ratio and aerosol scattering ratio from our Raman lidar data.

3. Experimental Results

The lidar data that we report on in this paper were acquired at the NASA Wallops Flight Facility, Virginia, on the Chesapeake Bay's eastern shore during the night of 9 September 1995. The primary purpose for the field deployment was to participate in an intercomparison of a number of different methods to measure atmospheric water vapor profiles. The methods included, in addition to the Raman lidar, a passive ground-based infrared interferometer and spectrometer[21]; two airborne differential absorption lidars, one on the NASA C-130 aircraft[22] and the other on the NASA ER-2 aircraft[23]; and several different operational humidity sensors carried aloft on standard radiosondes.

The lidar was located on the mainland approximately 3.2 km WNW of Wallops Island and acquired data for approximately 4.5 h, beginning at 00:10 UT (9:10 p.m. EDT 8 September 1995) and ending at 04:45 UT 9 September 1995. During the observation period the lidar was pointed sequentially, by means of the large mirror, at several angles. Because of the sequencing, we acquired 1-min profiles on the vertical once every 2 min. A radiosonde was launched at 02:33 UT 9 September 1995.

The skies over Wallops Island were generally clear when the lidar data acquisition was initiated. Shortly after 01:00 UT, clouds started to develop at three altitudes: 4 km, 3 km, and 400 m. At around 3:30 UT, another cloud deck appeared at an altitude of approximately 1 km.

An example of a water vapor mixing ratio profile obtained at 02:48 UT (2.80 h UT) near the middle of the observation period, is shown in Fig. 1. A single calibration constant relating the Raman-scattering ratio (Raman scattering by water vapor to nitrogen) to the water vapor mixing ratio was used to calibrate the lidar data shown in the figure. The calibration constant was obtained, following procedures outlined in Ferrare *et al.*,[6] from a best fit, over an altitude range of 2–6 km, of all 36 lidar–radiosonde sensor comparisons made during the entire field deployment (for the period 22 August to 21 September 1995).

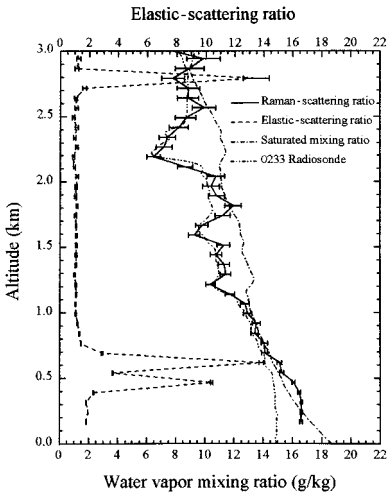

Fig. 1. Water vapor mixing ratio profile and an elastic-scattering ratio profile obtained with the scanning Raman lidar at the NASA Wallops Flight Facility on 9 September 1995 at 02:48 UT (2.80 h UT). Also shown is the water vapor mixing ratio and the saturated water vapor mixing ratio profiles made with data from the radiosonde launched at 02:33 UT.

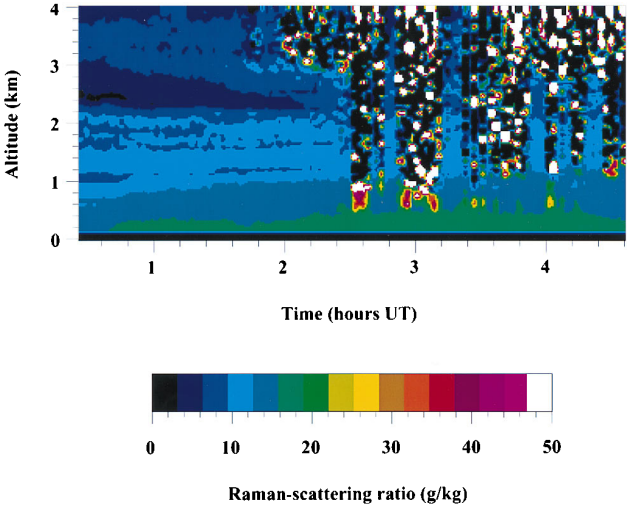

Fig. 2. False color, time–height image of the variation of the Raman-scattering ratio, normalized to the water vapor mixing ratio, during the night of 9 September 1995. The image is color coded as shown by the color bar.

The uncertainty bars shown on the lidar data represent an estimate of the one sigma standard error in the determination of the water vapor mixing ratio assuming that the lidar returns used to derive the ratio are Poisson distributed. The water vapor profile from the radiosonde launched at 02:33 UT (2.55 h UT) is shown in the figure for comparison. Also shown is the saturated water vapor mixing ratio profile. The saturated profile is calculated from the radiosonde temperature profile and corresponds to the expected water vapor mixing ratio at 100% relative humidity. We also show an elastic-scattering ratio profile acquired simultaneously with the water vapor profile at 2.80 h UT. The elastic-scattering ratio profile is normalized to unity in a typically clean region of the atmosphere extending in altitude from 6 to 10 km.[6] When this normalization scheme is used, a scattering ratio of unity is indicative of pure molecular scattering, whereas a scattering ratio in excess of one indicates the presence of aerosols or clouds.

The lidar measurement of the water vapor mixing ratio in the figure shows slight saturation over an altitude range from approximately 200 to 700 m. This corresponds to the altitude range where an optically thin cloud exists, as can be seen in the elastic-scattering ratio data (elastic-scattering ratios from 4 to 14) shown in the figure, an altitude region where optically dense clouds were coming and going. The lidar measurement also shows that the atmosphere was saturated between an altitude of 700 m and 1 km. In general, as shown in the figure, the lidar profile of the water vapor mixing ratio agrees well with the radiosonde measurement, especially above 1 km.

Over 120 independent vertical profiles of the Raman-scattering ratio and the elastic-scattering ratio as those shown in Fig. 1 were acquired by the lidar during the observation period. All of the vertical Raman-scattering ratio profiles acquired during the period have been combined together and are shown in the false color image of Fig. 2. Figure 2 shows a time–height image of the variation of the Raman-scattering ratio, normalized to the water vapor mixing ratio, during the night of 9 September 1995, color coded as shown by the color bar given in the figure. Prior to the onset of clouds at around 2.00 h UT, the image of Fig. 2 shows the layering of water vapor as a function of both height and time. Note that at 2.80 h UT in the color image we can see, in the vertical, changes of color that reveal the identical vertical structure of atmospheric moisture as presented in Fig. 1. The vertical stippling after 2.00 h UT—above an altitude of 3 km, and after 2.50 h UT—above 1 km are due to noise artifacts because of weak signals from strongly attenuating clouds. Occasionally, after 2.50 h UT, either because of the absence of clouds or because of low cloud optical depth, a measurement of the water vapor mixing ratio, with good signal to noise, can be made to altitudes above the clouds. Figure 2 shows these time periods to be at approximately 2.80 (data from this time period is shown in Fig. 1), 3.30, 3.90, 4.20, and 4.35 h UT.

All of the vertical elastic-scattering ratio profiles acquired during the observation period (over 120 profiles obtained simultaneously with the water vapor profiles) have been compiled in a similar false color image as the moisture data and are shown in Fig. 3. The high elastic-scattering ratio, in excess of 70, and shown as shades of red in Fig. 3, clearly delineate the location of clouds that were present during the observation period. We can see in the image of Fig. 3 the cloud layers that formed after the initiation of lidar data acquisition: First, broken clouds appeared at an altitude of approximately 4 km shortly after 1.00 h UT; then after 1.30 h UT a cloud deck developed at 3

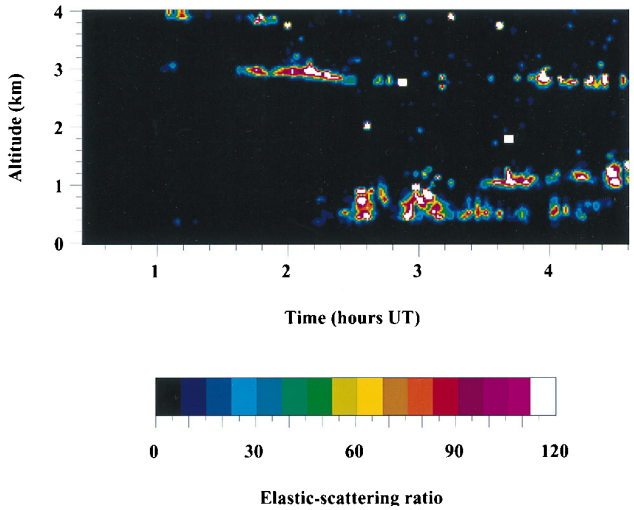

Fig. 3. False color, time–height image of the variation of the elastic-scattering ratio during the night of 9 September 1995, color coded as shown by the color bar.

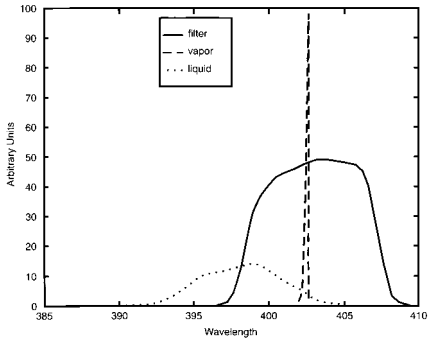

Fig. 4. The $\nu - 1$, $\nu - 3$ bands of bulk liquid water at 30 °C (combination of isotropic and anisotropic components) and the $\nu - 1$ band of water vapor excited by the 351.1-nm laser line are shown as a function of wavelength. The two bands (liquid and vapor) have been normalized so that their respective band strengths are in a ratio of 5:1. Also shown is the transmission curve for the interference filter used to select the Raman scattering.

km; at approximately 2.50 h UT, broken clouds with their base at approximately 400 m began to appear; finally, at 3.50 h UT a deck developed at 1 km. The stippled area in the upper right portion of Fig. 3, which is less obvious in this image, is also associated with noise that was due to the strong cloud attenuation.

The regions of apparently very high Raman-scattering ratio, in excess of 17 g/kg (water vapor mixing ratio equivalent), seen as the areas shaded in green, yellow, and red in the image of Fig. 2, cannot be due to atmospheric water vapor. We have already seen in the discussion of Fig. 1 that, in this altitude region, the saturation mixing ratio was less than 17 g/kg. Thus the air cannot hold more than 17 g/kg of water vapor. These regions can be seen in the image after approximately 2.50 h UT, ranging in altitude from approximately 400 m to 1 km. The images in Figs. 2 and 3 show that the regions of unrealistically high water vapor mixing ratio are correlated closely with the locations of clouds. We suggest that this excess scattering in the Raman water vapor detector channel is due to Raman scattering by cloud droplets, and this is discussed in more detail in the next two sections.

4. Raman Scattering by Water Droplets

Raman scattering by bulk liquid water has been reported by a number of investigators (see Ref. 24). The $\nu - 1$, $\nu - 3$ band of bulk liquid water[24] and the $\nu - 1$ band of water vapor[25] excited by the 351.1-nm laser line are shown in Fig. 4. Laboratory measurements indicate that the band strength per molecule (integrated cross section) for Raman scattering by bulk liquid water ($\approx 4.5 \pm 0.3 \times 10^{-29}$ cm^2 sr^{-1})[26] is approximately five times the band strength for water vapor ($\approx 7.90 \times 10^{-30}$ cm^2 sr^{-1}).[27] The two bands (liquid and vapor) are shown in the figure with a band strength ratio of five to one. The spectral location of the peak of the $\nu - 1$ Raman water vapor band is shifted relative to the incident radiation by a frequency of 3652 cm^{-1} (Ref. 28). This corresponds to a Raman wavelength of 402.7 nm when excited at the 351.1-nm laser line, as seen in Fig. 4. As can be seen in the figure, the liquid band is much broader than the vapor band, is shifted from the exciting line less than the vapor band, and, to some degree, overlaps the vapor band. Because the excimer laser output is unpolarized, we have combined the isotropic and anisotropic bands together to derive the resultant Raman liquid band which is shown in the figure. The shape of the Raman liquid band varies with temperature. We show in the figure the resultant liquid band for a temperature of 30 °C.

Also shown in Fig. 4 is the transmission curve for the interference filter used to select the Raman scattering by water vapor. As mentioned above, the excimer laser has two additional lines centered around the central line at 348.8 and 353.2 nm. Each of these satellite laser lines also produce Raman bands by liquid water and water vapor similar to but slightly shifted in wavelength when compared with the bands shown in Fig. 4. The location of the peak of the $\nu - 1$ Raman water vapor band excited by the laser lines at 348.8 and 353.2 nm are at 399.7 and 405.5 nm, respectively. The wide bandpass of the interference filter used in the investigation, and shown in the figure, was selected to pass the three water vapor bands from the three laser lines. As can be seen in Fig. 4, the filter also passes a portion of the liquid water band.

In clouds, we expect Raman scattering, not from bulk water, but from water droplets. Both stimulated and spontaneous Raman scattering[11] by water droplets have been observed in the laboratory. As mentioned in the introduction, very high intensities,[15,16] greater than 0.1 GW cm^{-2}, are required to produce stimulated Raman scattering by droplets. At an altitude of 400 m (typical cloud base during this experiment), the instantaneous intensity of the exci-

mer laser used in the investigation was less than 5.0 kW cm^{-2}, much less than that required for simulated Raman scattering. Thus we limit our discussion to spontaneous Raman scattering by droplets.

It is the interaction between the laser radiation that enters the droplets and the liquid water molecules that produces spontaneous Raman scattering. We expect, then, that the scattering will be proportional to the liquid content of the droplet, modified by the characteristics of the droplet itself. The shape of the Raman-scattering phase function and the backscatter cross section of the droplets will depend on the effect that the spherical shape and size of the droplets have on (1) the intensity of the incident radiation within the droplets, (2) the Raman conversion process within the droplets, (3) the efficiency with which the Raman-shifted radiation exits the droplets, and (4) the pattern that this process produces.

Kerker and Druger[29] have theoretically studied the scattering phase function for a uniform distribution of wavelength-shifting, scattering dipoles embedded within a sphere. They used Mie theory to predict the internal intensity of the incident radiation within a sphere of index m and then they calculated the scattering phase function (wavelength shift = 1.196 λ) external to the sphere that was due to a single scatterer embedded inside the sphere. They then used a superposition of solutions to calculate the scattering phase function that was due to a uniform distribution of scatterers within the sphere. They looked at several different-sized spheres (α = 0.1 to 20) and several indices of refraction (m = 1.10, 1.20, 1.33, and 1.50) using the dimensionless size parameter defined as $\alpha = 2\pi a/\lambda$, which relates the radius of the sphere a to the wavelength of the incident radiation λ. They found for small spheres, α = 0.2, that the scatterers act like a collection of dipoles whose scattering phase function is similar in shape to that expected from a collection of independently scattering molecules. For larger spheres they found that, as the size of the spheres become more important, the scattering phase function becomes peaked in the backscatter direction (180°). For a sphere of index m = 1.50, they found that the backscatter cross section for size parameter α = 6 and 8 is enhanced by a factor of approximately 2 and 3, respectively, when compared with the cross section at other angles (They do not provide the scattering phase function for a water sphere of index 1.33.) Although the authors caution that each sphere size must be studied individually, it is obvious that for larger spheres there tends to be an enhancement of the backscatter cross section.

One effect of the sphere size on Raman scattering is referred to as structural resonances. The resonances are a function only of the size parameter of the sphere and result from singularities in the expansion coefficients of the internal field as predicted by Mie theory. These resonances are expected to occur for both the incident and the Raman-shifted radiation. Thurn and Kiefer[11] provide an overview of the expected Mie intensities within the sphere. When the resonances occur with the incident radiation, the effect is to increase the internal intensity of the incident light at the resonant wavelength and thus increase the effective cross section for Raman scattering within the sphere when compared with Raman scattering by bulk water. In the present experiment we would expect these resonances to occur for each of the three laser lines with the appropriate size cloud droplets. We know that clouds are made up of droplets distributed over a range of radii from approximately 1 to 15 μm.[30] Thus we might expect a large number of resonances to occur in a typical cloud.

As mentioned above, we also expect resonances to occur with the Raman-shifted radiation. If we assume that the resonances in the Mie solution[11] represent normal modes of the droplets, then each cloud droplet (at a given radius) would have a number of resonances with the Raman-shifted radiation since that radiation is spectrally broad, as seen in Fig. 4. The effect of these resonances would be to also increase the effective Raman cross section at the resonance frequencies. The second of these two resonances has been studied by Thurn and Kiefer.[11] Their research on a water-glycerol droplet has shown that the cross section for Raman scattering by the water band of the droplets is similar in shape to bulk water but has sharp lines superimposed, which is attributed to Raman-shifted resonances. Their laboratory work was performed on a single droplet so that they were not able to observe resonances associated with the incident laser wavelength. Schweigar[12] studied Raman scattering from a pure water droplet. He observed Raman scattering at a scattering angle of approximately 90 degrees from a single levitated droplet over a period of several hours as the droplet evaporated. He was able to observe both types of resonant scattering by the water droplet in addition to nonresonant scattering. He showed that, although the Raman cross section of a single sphere can change by as much as an order of magnitude between resonant and nonresonant scattering (resulting from a very small change in size parameter), if the scattering is averaged over a range of size parameters then the mean scattered intensity is proportional to the droplet volume, or to the total liquid content of the sphere. His laboratory data show that the scattered intensity at 90 degrees, including effects of the resonances, was approximately a factor of 2 greater than the assumed nonresonant scattered intensity.

In summary, as a result of the above discussion, we can expect that the Raman backscatter cross section of a distribution of droplets may be proportional to the total liquid water contained in the droplets. Furthermore, we can expect that the droplet backscatter cross section will be significantly larger than the backscatter cross section of the equivalent number of water vapor molecules in the vapor phase. A quantitative estimate of the effective Raman backscatter cross section for a realistic distribution of cloud droplets (a = 1 to 15 μm or α = 18 to 268 at λ = 351.1 nm) has not yet been attempted.

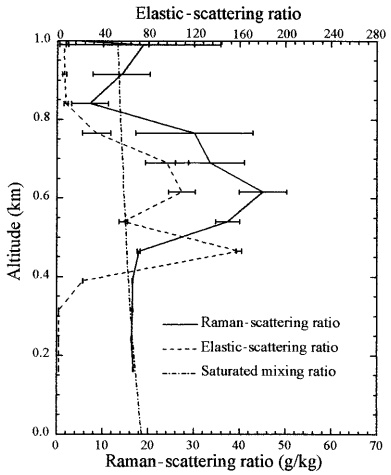

Fig. 5. Profiles of the Raman-scattering ratio, normalized to the water vapor mixing ratio, and the elastic-scattering ratio acquired at 3.13 h UT. The elastic-scattering ratio refers to the upper scale. Also shown is the saturated mixing ratio (100% relative humidity) profile obtained with the temperature data from the 02:33 UT radiosonde. The Raman-scattering ratio and the saturated mixing ratio are plotted in reference to the bottom scale.

5. Discussion

As was mentioned above, Fig. 2 shows a number of regions where the Raman-scattering ratio, when normalized to the water vapor mixing ratio, exceeds that which would be associated with saturated air. The regions in question are shown as areas shaded in green, yellow, and red in Fig. 2 and range in altitude from approximately 500 m to 1 km. They appear as (1) a large feature extending from approximately 2.50 to 2.60 h UT, (2) a three-lobed feature extending from approximately 2.80 to 3.20 h UT, (3) four small features centered at 3.45 h UT, and (4) another small feature at 4.00 h UT. Note that, from the color bar, the peak value of water vapor mixing ratio equivalent within the regions of interest vary between 20 and 50 g/kg. We now look at several of these features in more detail.

Shown in Fig. 5 are profiles of the Raman-scattering ratio and the elastic-scattering ratio acquired at 3.13 h UT, which is through the center of the third lobe of the three-lobed feature of Fig. 2. The saturated mixing ratio (100% relative humidity) profile obtained with the temperature data from the 02:33 UT radiosonde is also shown in the figure.

From the elastic-scattering ratio shown in the figure, we can see an indication of clear air (elastic-scattering ratio = 1) to an altitude of approximately 400 m. Between 400 and 800 m we observe a cloud that appears as two layers: the lower layer peak is at 500 m and a second peak of smaller amplitude at an altitude of 600 m. The elastic-scattering ratio then returns to a clear air level at an altitude of approximately 800 m. The Raman-scattering ratio data given in the figure are consistent with a reasonable water vapor mixing ratio below an altitude of 400 m (near saturation). Above 400 m, the Raman-scattering ratio starts to increase gradually to an altitude of 500 m, then more sharply to a peak value of 45 g/kg water vapor equivalent at an altitude of 600 m. The Raman-scattering ratio then falls off to a level that is consistent with a saturated water vapor mixing ratio value at approximately 800 m, an altitude just at cloud top. The difference between the saturated mixing ratio as measured by the radiosonde and the Raman-scattering ratio (at the peak, approximately 45 g/kg − 15 g/kg = 30 g/kg) is attributed to Raman scattering by cloud droplets. The peak in the cloud droplet signal appears to be correlated with the upper peak in the elastic-scattering ratio at an altitude of 600 m. Above cloud base both the aerosol and the Raman signals have a higher standard error, as indicated by the increased length of the error bars. The higher standard error is due to the large attenuation by the cloud, of the outgoing laser beam, and the returned scattered radiation.

Two additional examples comparing simultaneously the acquired elastic-scattering ratio and the Raman-scattering ratio measurements are shown in Figs. 6 and 7. The data of Fig. 6 were obtained at 2.90 h UT through the first lobe of the three-lobed feature of Fig. 2. The example shown in Fig. 7 was acquired at 3.00 h UT through the middle lobe of the three-lobe feature. In the data of both Figs. 6 and 7 we can again see a strong correlation between the upper peak in the elastic-scattering ratio and the peak in the Raman-scattering ratio. Note that in Fig. 7 the lower cloud layer as seen in the elastic-scattering ratio profile is reduced significantly in intensity when compared with the other examples. Again, in these two examples the two scattering ratios are consistent with clear air conditions, within experimental error, both above and below the cloud.

The three examples presented above were chosen because the attenuation that is due to the clouds was sufficiently low that the standard error of both profiles, in each example, above cloud top would allow for a meaningful measurement of the clear sky conditions.

A fourth example is given in Fig. 8. The data of Fig. 8 were acquired at 2.53 h UT through the center of the large cloud feature of Fig. 2. This cloud had the highest optical depth of any observed on the night of the experiment. The two scattering ratio profiles are again consistent with clear conditions below the cloud. In the upper level of the cloud and above, the standard error is too large to provide reliable ratios as can be seen by the very large error bars at around 800 m. We again can see an altitude correlation between the two scattering ratios in the upper layer of the cloud.

We know from the discussion of Section 4 that, in the laboratory, Raman scattering from a water droplet when averaged over a size range is proportional to liquid water content. We suggested, as a natural extension, that the Raman backscatter cross section of a distribution of droplets may be proportional to the total liquid water contained in the droplets. If we now assume that the observed Raman scattering is proportional to cloud liquid water in this experiment, then the four examples presented above would be consistent with a cloud of two distinct layers: the

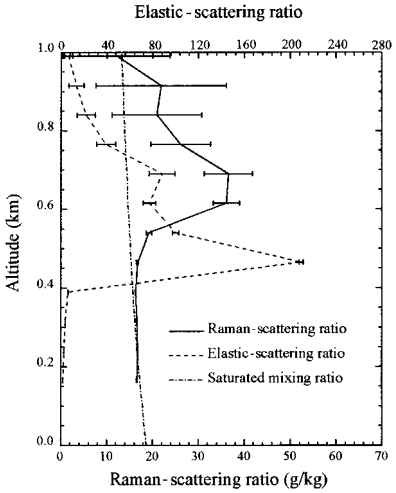

Fig. 6. Same as Fig. 5, except that the Raman-scattering ratio and the elastic-scattering ratio were acquired at 2.90 h UT.

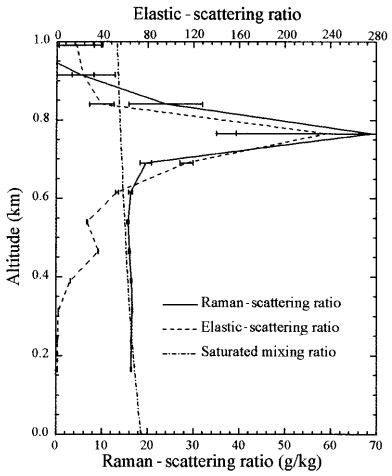

Fig. 7. Same as Fig. 5, except that the Raman-scattering ratio and the elastic-scattering ratio were acquired at 3.00 h UT.

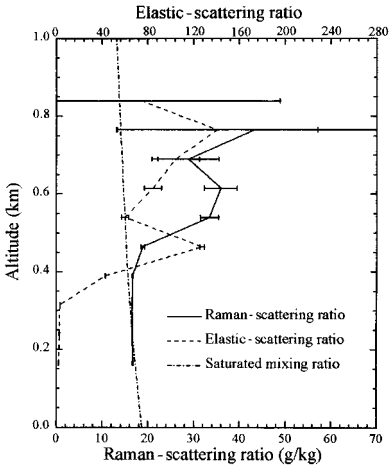

Fig. 8. Same as Fig. 5, except that the Raman-scattering ratio and the elastic-scattering ratio were acquired at 2.53 h UT.

lower with low liquid water and the upper with higher liquid water. The lower layer could be a haze with a large number of small droplets, giving rise to high Mie scattering, but with low liquid water, and thus small Raman scattering from the liquid in the droplets. The upper layer could have a distribution of larger droplets, possibly closer to a typical cumulus cloud, giving rise to a high value for both the elastic-scattering ratio and the Raman-scattering ratio. Without *in situ* measurements of the microphysical properties of the clouds, this description of the clouds, of course, cannot be confirmed.

We have identified two reasons that Raman lidar observations of real clouds may not be related linearly to cloud liquid water. One reason is multiple scattering. The impact of multiple scattering, due to the presence of clouds, in Raman lidar measurements has been studied theoretically.[31] It was shown that the increased backscatter that is due to multiple scattering is essentially the same for the Raman wavelengths used to derive both the water vapor mixing ratio and the elastic-scattering ratio, thus the effect is nearly canceled when the ratio is calculated. The small residual, due to the difference in the Mie-scattering cross section at the two scattered wavelengths, amounts to only a few percent error in the ratio. However, there may be an additional factor that is due to the unknown scattering phase function of Raman scattering by the liquid droplets. The error in the ratio introduced by this factor is also likely to be small, but cannot be evaluated until we have estimated the scattering phase function for a realistic distribution of cloud-sized droplets. The second reason is a possible variation in scattering phase function as a function of size for cloud-sized droplets. We remember from Section 4 that, for very small droplets ($\alpha = 0.2$), the water molecules in the droplet act as independent scatterers with a scattering phase function similar to that of molecules. For larger droplets ($\alpha = 6$ or 8) we found that the phase function was enhanced at 180° by approximately a factor of 2 or 3, respectively. The laboratory work of Schweigar[12] investigating Raman scattering by a single water droplet indicates that this variation is likely to be small. However, a full evaluation of this effect in real clouds will also have to await our estimate of the Raman-scattering phase functions of cloud droplets.

Let us now estimate the magnitude of the enhancement that is due to the spherical shape of the droplets. Figure 5 shows a peak value for the Raman scattering from the cloud droplets, which, as mentioned above, is the difference between the Raman-scattering ratio and the saturated mixing ratio, at an altitude of 600 m to be approximately 30 g/kg water vapor equivalent (45 − 15 g/kg = 30 g/kg). We know that the typical liquid water content of these low-level clouds is a few tenths of a gram per kilogram.[30] Thus, if we assume a liquid water mixing ratio between 0.6 and 0.3 g/kg, there is a difference of a factor of 50 and 100 between the measured per molecule signal from the cloud droplets and the total number of water molecules in the liquid state, respectively. This difference can be explained by a combination of four factors: (1) the difference in sensitivity of the Raman water channel to the Raman-scattered radiation from vapor and liquid, (2) the difference in Raman cross section of water molecules in the vapor and the liquid state, (3) the expected enhancement in Raman backscatter cross section that is due to the spherical shape of the droplets described in Section 4, and (4) the average effect of the structural resonances on the scattering cross section. The first two factors can account for approximately 50% of the difference. Figure 4 shows that the filter passes approximately 50% of the Raman water vapor band (note the filter transmission at the spectral location of the water vapor band) and only approximately 20% of the liquid water band (an overlap of the liquid water band and the filter transmission curve). Thus these two factors cause the

Raman signal from liquid water molecules to be about twice that from vapor molecules on a per molecule basis. Therefore, to account for the magnitude of the observed Raman backscatter from the cloud droplets, the enhancements that are due to the spherical shape of the droplets must be in the range between 25 and 50. In reference to the third factor mentioned above, we found in Section 4 that the scattering phase function of a sphere of index 1.5 and size parameter $\alpha = 8$ is peaked in the backscatter direction with approximately three times more scattering at 180° than at other angles. This would reduce the unexplained enhancement to a range of between 8 and 16. Finally, in reference to factor four mentioned above, we also know from our discussion of Section 4 that at 90° the average structural resonance effects can account for a scattering increase of approximately 2. This then leaves the unexplained enhancement of Raman scattering from droplets to be in the range of 4 and 8. What can account for the unexplained enhancement? There are a number of factors that might account for the remaining unexplained enhancement. These are: (1) the uncertainty in the absolute Raman cross section of water vapor and bulk water, (2) the magnitude of backscatter enhancement for spheres of index 1.33 and spheres larger than $\alpha = 8$, (3) the average effect of the structural resonances for a scattering angle of 180°, and (4) uncertainty in the magnitude of the nonresonant component of droplet scattering. A full evaluation of the enhancement will have to await a quantitative study of Raman scattering by a real distribution of cloud droplets.

There are two instrumental effects that we have identified that might produce enhanced signals in the presence of clouds, which we have interpreted to be Raman scattering from cloud liquid droplets: (1) bleed through of the strong cloud scattering at the laser wavelength (351 nm) through the water vapor filter that is centered at 402 nm, and (2) signal-induced noise (SIN) in the PMT's. Each of these are discussed separately.

The interference filters that select the Raman bands were manufactured with extra blocking at the laser wavelength (approaching 10^{-12}) to avoid the possibility of bleed through. However, the more convincing argument that bleed through is not the cause of the observed Raman scattering from clouds can be seen in Figs. 5, 6, 7, and 8. As the profiles given in the four figures show, the shape of the elastic-scattering ratio and the Raman-scattering ratio from the clouds are very different. If bleed through were a significant source of the apparent Raman scattering from cloud droplets, we would expect a similar shape in the profiles. Thus we do not believe that bleed through is a major source of the Raman signal that we have observed.

SIN is normally expected to be a problem when a weak light signal is being sensed by a PMT after a relatively strong light was incident on the PMT,[32] a situation that exists in this experiment. The initial light level incident onto the PMT before the low-level cloud is 2 to 3 orders of magnitude stronger than the scattered light coming from within and above the cloud. If SIN were a significant problem within the cloud we would expect that it would be an even greater problem in the clear atmosphere above the cloud. The profiles given in Fig. 5, 6, and 7 show that, to within experimental error, the Raman-scattering ratio and the elastic-scattering ratio above the clouds are consistent with the clear air expected levels. Thus we believe that there is no significant SIN within the clouds, where we are observing a higher signal level associated with the Raman scattering from the cloud droplets, than the signal from the atmosphere above, where no SIN is observed.

6. Summary and Conclusions

We reported in this paper on the observation of Raman scattering by liquid water in cloud droplets. The NASA Goddard Space Flight Center scanning Raman lidar participated in a water vapor intercomparison study at the NASA Wallops Flight Facility during the months of August and September 1995. During the night of 9 September 1995, Raman scattering in the water vapor channel well in excess of 100% relative humidity was observed from low-level clouds. The excess scattering has been interpreted to be spontaneous Raman scattering from liquid water in the cloud droplets. We believe that our lidar was able to observe this effect because of the spectrally wide interference filter used to select Raman scattering by water vapor from the three output frequencies of our excimer laser. Because of the width of the filter there is good overlap of the filter transmission and the spectrally broad Raman liquid water band.

A review of theoretical and laboratory studies of spontaneous Raman scattering by spheres indicates that there are structural resonances, due to the spherical shape of the droplets, that will enhance the Raman backscatter cross section of molecules in the sphere. Furthermore, the laboratory investigations demonstrate that Raman scattering from spheres distributed in size, which tends to average the effect of the resonances, is proportional to the volume of the spheres. As a result of these laboratory studies, Raman scattering by cloud droplets, which are also distributed in size, may provide a new remote method to study cloud liquid water content.

A factor of 25–50 enhancement in Raman scattering from the cloud droplets is required to make the Raman-scattering observations reported here consistent with the expected concentration of cloud liquid water. A backscatter enhancement that is due to the spherical shape of the droplets and a laboratory measured average effect of the structural resonances (scattering angle of 90°) can only account for approximately a factor of 6. This leaves a range of unexplained enhancement of between 4 and 8. We mention four possibilities that might account for the remaining unexplained enhancement. They were (1) the uncertainty in the absolute Raman cross section of water vapor and bulk water, (2) the magnitude of backscatter enhancement for spheres of index 1.33 and spheres larger than $\alpha = 8$, (3) the average effect

of the structural resonances for a scattering angle of 180°, and (4) uncertainty in the magnitude of the nonresonant component of droplet scattering. A quantitative estimate of the Raman backscatter cross section for a realistic distribution of cloud droplets has not yet been attempted.

The Raman-scattering profile by cloud droplets was significantly different from the simultaneously acquired elastic-scattering profile by the same clouds. An evaluation of both the aerosol scattering ratio and the Raman-scattering ratio profiles of the clouds studied seems to suggest that the clouds had two distinct layers: a lower layer that might consist of a small droplet haze and an upper layer that is more consistent with a large droplet distribution.

In conclusion, we believe that the combined observation of Raman scattering and Mie scattering by cloud droplets has the promise to lead to new methods for the remote study of cloud liquid water and cloud droplet size distribution. In the meantime, care should be exercised with the use of Raman lidar to derive the water vapor mixing ratio in the presence of clouds because of possible interference due to Raman scattering by liquid water, especially if the lidar utilizes a spectrally wide interference filter in the water vapor channel.

References

1. S. H. Melfi, D. N. Whiteman, and R. Ferrare, "Observation of atmospheric fronts using Raman lidar moisture measurements," J. Appl. Meteorol. **28,** 789–806 (1989).
2. A. Ansmann, M. Riebesell, U. Wandinger, C. Weitkamp, E. Voss, W. Lahmann, and W. Michaelis, "Combined Raman elastic-backscatter lidar for vertical profiling of moisture, aerosol extinction, backscatter, and lidar ratio," Appl. Phys. B **55,** 18–28 (1992).
3. D. N. Whiteman, S. H. Melfi, and R. A. Ferrare, "Raman lidar system for the measurement of water vapor and aerosols in the Earth's atmosphere," Appl. Opt. **31,** 3068–3082 (1992).
4. J. E. M. Goldsmith, S. E. Bisson, R. A. Ferrare, K. D. Evans, D. N. Whiteman, and S. H. Melfi, "Raman lidar profiling of atmospheric water vapor: simultaneous measurements with two collocated systems," Bull. Am. Meteorol. Soc. **75,** 975–982 (1994).
5. R. A. Ferrare, S. H. Melfi, D. N. Whiteman, K. D. Evans, F. J. Schmidlin, and D. O'C. Starr, "A comparison of water vapor measurements made by Raman lidar and radiosondes," J. Atmos. Ocean. Technol. **12,** 1177–1195 (1995).
6. R. A. Ferrare, S. H. Melfi, D. N. Whiteman, and K. D. Evans, "Raman lidar measurements of Pinatubo aerosols over southeastern Kansas during November-December 1991," Geophys. Res. Lett. **19,** 1599–1602 (1992).
7. R. A. Ferrare, D. N. Whiteman, and S. H. Melfi, "Raman lidar measurements of temperature in the troposphere and lower stratosphere," in *Optical Remote Sensing of the Atmosphere*, Vol. 4 of 1990 OSA Technical Digest Series (Optical Society of America, Washington, D.C., 1990), pp. 188–191.
8. K. D. Evans, S. H. Melfi, R. A. Ferrare, and D. N. Whiteman, "Upper tropospheric temperature measurements using a Raman lidar," Appl. Opt. **36,** 2594–2602 (1997).
9. C. R. Philbrick, F. J. Schmidlin, K. U. Grossman, G. Lange, D. Offerman, K. D. Baker, D. Krankowsky, and U. von Zahn, "Density and temperature structure over Northern Europe," J. Atmos. Terr. Phys. **47,** 159–172 (1985).
10. G. Vaughan, D. P. Wareing, S. J. Pepler, L. Thomas, and V. Mitev, "Atmospheric temperature measurements made by rotational Raman scattering," Appl. Opt. **32,** 2758–2764 (1993).
11. R. Thurn and W. Kiefer, "Structural resonances observed in the Raman spectra of optically levitated droplets," Appl. Opt. **24,** 1515–1519 (1985).
12. G. Schweigar, "Raman scattering on microparticles: size dependence," J. Opt. Soc. Am. B **8,** 1770–1778 (1991).
13. R. G. Pinnick, A. Biswas, R. L. Armstrong, H. Latifi, E. Creegan, V. Srivastava, and G. Fernandez, "Stimulated Raman scattering in micrometer-sized droplets: measurements of angular scattering characteristics," Opt. Lett. **12,** 1099–1101 (1988).
14. V. Srivastava and M. A. Jarzembski, "Laser-induced stimulated Raman scattering in the forward direction of a droplet: comparison of Mie theory with geometrical optics," Opt. Lett. **16,** 126–128 (1991).
15. A. Serpenguzel, J. C. Swindal, R. K. Chang, and W. P. Acker, "Two-dimensional imaging of sprays with fluorescence, lasing, and stimulated Raman scattering," Appl. Opt. **31,** 3543–3551 (1992).
16. A. Serpenguzel, G. Chen, R. K. Chang, and W.-f. Hsieh, "Heuristic model for the growth and coupling of nonlinear processes in droplets," J. Opt. Soc. Am. B **9,** 871–883 (1992).
17. D. H. Leach, R. K. Chang, W. P. Acker, and S. C. Hill, "Third-order sum-frequency generation in droplets: experimental results," J. Opt. Soc. Am. B **10,** 34–45 (1993).
18. R. J. Charlson, S. E. Schwartz, J. M. Hales, R. D. Cess, J. A. Coakley, J. E. Hansen, and D. J. Hofmann, "Climate forcing by anthropogenic aerosols," Science **255,** 423–430 (1992).
19. D. N. Whiteman, W. F. Murphy, N. W. Walsh, and K. D. Evans, "Temperature sensitivity of an atmospheric Raman lidar system based on a XeF excimer laser," Opt. Lett. **18,** 247–249 (1993).
20. S. H. Melfi, "Remote measurements of the atmosphere using Raman scattering," Appl. Opt. **11,** 1605–1610 (1972).
21. A. D. Collard, S. A. Ackerman, W. L. Smith, X. Ma, H. E. Revercomb, R. O. Knuteson, and S.-C. Lee, "Cirrus cloud properties derived from high spectral resolution infrared spectrometry during FIRE II. Part III. Ground-based HIS results," J. Atmos. Sci. **52,** 4264–4275 (1995).
22. N. S. Higdon, E. V. Browell, and P. Ponsardin, "Airborne differential absorption lidar system for measurements of atmospheric water vapor and aerosols," Appl. Opt. **33,** 6422–6438 (1994).
23. S. Ismail and E. V. Browell, "Airborne and spaceborne lidar measurements of water vapor profiles: a sensitivity analysis," Appl. Opt. **28,** 3603–3614 (1989); **28,** 4981(E) (1989).
24. J. R. Scherer, M. K. Go, and S. Kint, "Raman spectra and structure of water from −10 to 90°," J. Phys. Chem. **78,** 1304–1313 (1974).
25. W. F. Murphy, "The rovibrational Raman spectrum of water vapour ν_1 and ν_3," Mol. Phys. **36,** 727–732 (1978).
26. R. B. Slusher and V. E. Derr, "Temperature dependence and cross sections of some Stokes and anti-Stokes Raman lines in ice lh," Appl. Opt. **14,** 2116–2120 (1975).
27. A. Weber, *Raman Spectroscopy of Gases and Liquids*, Vol. 11 of Topics in Current Physics (Springer-Verlag, Berlin, 1979).
28. W. A. Senior and W. K. Thompson, "Assignment of the infrared and Raman bands of liquid water," Nature (London) **205,** 170 (1965).
29. M. Kerker and S. D. Druger, "Raman and fluorescent scattering by molecules embedded in spheres with radii up to several multiples of the wavelength," Appl. Opt. **18,** 1172–1179 (1979).
30. R. R. Rogers and M. K. Yau, *A Short Course in Cloud Physics*, 3rd ed. (Pergamon, Oxford, 1989).
31. U. Wandinger, "Influence of multiple scattering on DIAL, Raman, and high spectral resolution lidars—a common MUSCLE study," in *Abstract Book, 18th International Laser Radar Conference* (International Committee for Laser Atmospheric Studies, Berlin, Germany, 1996), p. 80.
32. C. J. Grund and E. W. Eloranta, "University of Wisconsin high spectral resolution lidar," Opt. Eng. **30,** 6–12 (1991).